Chinese Journal of Aeronautics, (2022), 35(11): 45–58

Chinese Society of Aeronautics and Astronautics
& Beihang University

Chinese Journal of Aeronautics

cja@buaa.edu.cn
www.sciencedirect.com

Revisiting the space-time gradient method: A time-clocking perspective, high order difference time discretization and comparison with the harmonic balance method

Boqian WANG [a], **Dingxi WANG** [a], **Mohammad RAHMATI** [b], **Xiuquan HUANG** [a,*]

[a] *School of Power and Energy, Northwestern Polytechnical University, Xi'an 710072, China*
[b] *Department of Mechanical and Construction Engineering, Northumbria University, Newcastle upon Tyne NE1 8ST, United Kingdom*

Received 27 September 2021; revised 21 October 2021; accepted 27 October 2021
Available online 6 June 2022

KEYWORDS

Harmonic balance method;
High order difference scheme;
Passage reordering;
Space-time gradient method;
Unsteady flows

Abstract This paper revisits the Space-Time Gradient (STG) method which was developed for efficient analysis of unsteady flows due to rotor–stator interaction and presents the method from an alternative time-clocking perspective. The STG method requires reordering of blade passages according to their relative clocking positions with respect to blades of an adjacent blade row. As the space-clocking is linked to an equivalent time-clocking, the passage reordering can be performed according to the alternative time-clocking. With the time-clocking perspective, unsteady flow solutions from different passages of the same blade row are mapped to flow solutions of the same passage at different time instants or phase angles. Accordingly, the time derivative of the unsteady flow equation is discretized in time directly, which is more natural than transforming the time derivative to a spatial one as with the original STG method. To improve the solution accuracy, a ninth order difference scheme has been investigated for discretizing the time derivative. To achieve a stable solution for the high order scheme, the implicit solution method of Lower-Upper Symmetric Gauss-Seidel/Gauss-Seidel (LU-SGS/GS) has been employed. The NASA Stage 35 and its blade-count-reduced variant are used to demonstrate the validity of the time-clocking based passage reordering and the advantages of the high order difference scheme for the STG method. Results from an exist-

* Corresponding author.
E-mail address: xiuquan_huang@nwpu.edu.cn (X. HUANG).
Peer review under responsibility of Editorial Committee of CJA.

Production and hosting by Elsevier

https://doi.org/10.1016/j.cja.2022.05.016

ing harmonic balance flow solver are also provided to contrast the two methods in terms of solution stability and computational cost.

1. Introduction

Computational Fluid Dynamics (CFD) has been an essential tool for modern turbomachinery design for many decades. The steady Mixing-Plane (MP) approach[1] has so far been widely used for analyzing the steady or time averaged flow field within multiple blade-rows in routine designs. The method has a fast turnaround but ignores the inherent unsteady characteristics in turbomachinery flow field. Modern advanced turbomachines are designed to have high loading and compact structure, resulting in intensified unsteady flow features even at the design operating condition. To meet the design challenge, there is even a need to assess the impact of unsteadiness on the aerodynamic performance at the design operating point.

The Dual Time Stepping (DTS) method[2] proposed by Jameson in 1991 is a general and classic unsteady solution method, but its time and memory consumption tends to be 2 to 3 orders of magnitude more than the MP approach[3] in the context of turbomachinery applications. This renders the inapplicability of the DTS method for daily design activities. Fortunately, the inherent unsteady flow field in turbomachinery is often characterized by unique and predetermined temporal and spatial periodicities, largely thanks to the cyclic symmetry of turbomachinery structures. The temporal and spatial periodicities have long been exploited to develop efficient reduced order methods for analyzing turbomachinery unsteady flows.

With the spatial periodicity, spatial truncation is often applied to reduce the number of passages in a computational domain. A truncated domain often consists of one blade passage per blade row and the phase shift boundary condition must be applied along the geometrically periodic boundaries in the lateral direction. The direct store method[4] and the shape correction method[5] are the typical time domain reduced order methods using truncated domains. With temporal periodicity, unsteady flow can be represented using a truncated Fourier series. This transforms the original unsteady flow equations to quasi-steady flow equations, leading to fast solution convergence. The typical reduced order methods include the Harmonic Balance (HB) method[6–8] and the nonlinear harmonic method.[9] Note that these reduced order methods also use truncated domains for turbomachinery applications.

To apply the reduced order methods to unsteady flows due to blade row interaction, one of the major challenges is how to treat the interface between a rotor–stator interface. An interface treatment will not only influence solution convergence, but also affect solution accuracy. A good interface treatment should have tight flux conservation and is non-reflective. Unfortunately, domain truncation makes it hard to design an interface treatment which satisfies the two requirements.

Recently, Yi et al. developed an efficient reduced order method for analyzing blade row interaction unsteady flow—the Space-Time Gradient (STG) method.[10–11] Different from all existing reduced order methods, it does not truncate computational domain. Therefore, it can use the sliding plane method which is developed for a time domain full order method. The temporal flow variation at a given point in a blade passage is linked to the flow variation of corresponding points in different passages at the same time using temporal and spatial periodicities of turbomachinery unsteady flows. It has been demonstrated that the STG method has the same convergence characteristic as the frozen rotor method. However, it can capture the unsteadiness due to blade row interaction with good accuracy at a time cost comparable to that of the frozen rotor method.

The STG method replaces the original time derivative with a spatial derivative. The spatial derivative is calculated using a backward second order finite difference method. Passage reordering is required to find the relevant passages for performing finite differencing. The STG method performs passage reordering based upon the relative spatial clocking in the circumferential direction: all blade passages of the same row are ordered according to their relative lateral clocking positions with respect to their nearest blades from the other blade row.

This paper revisits the STG method and presents the method from a time-clocking perspective. For a blade row interaction, it is well known that the unsteady flow fields of different passages from the same row have the same magnitude but different phases. The phase difference between adjacent blade passages is called inter blade phase angle and is known beforehand. The known phases of flow field provide the needed information for phase/time clocking. Rather than convert the time derivative of the original unsteady flow governing equation to a spatial derivative, we want to maintain the use of time derivative. To do this, the flow fields of different passages of the same row are mapped to flow fields of the same passage at different time instants according to the known inter blade phase angle. To use a finite difference scheme for the time derivative calculation, we also need to reorder the flow fields of different passages. The passage reordering can be performed based upon the phases of flow fields at different passages of the same row. It is not difficult to understand that the raw phases of flow fields of different passages can be bigger than 360°. For the passage reordering, the first step is to bring all the phases to the range of [0°,360°). This can be achieved by simply adding multiple of 360° to the raw phases if they are less than zero or subtracting multiple of 360° from the raw phases if they are no smaller than 360°. Hereafter we can order the passages according to the regulated phases in an ascending order. We can see that the phase angle based reordering does not require the knowledge of blade geometry. The only thing needed is the blade counts of two blade rows being involved and relative rotation direction, as they are required to obtain the inter blade phase angle and calculate the raw phases of different blade passages. It should be noted that the time /phase-clocking based passage reordering is essentially the same as the original passage reordering which is based upon space-

clocking, as the phase angle is simply a weighted time (weighted by the blade passing angular frequency) and the time and space clockings have one to one correspondence. Therefore, the passage reordering results by these two methods will be the same as expected.

Apart from the time-clocking perspective of the STG method, a high order difference scheme for time discretization is also investigated in this study. The high order scheme is well needed for cases where the number of passages of a blade row is small, to maintain acceptable solution accuracy without incurring dramatic computational cost overhead. Quite often high order schemes are prone to solution instability. To ensure a stable solution with a high order difference scheme, an implicit solution method is proposed with the consideration of easy implementation.

The paper is organized as follows. First the original STG method is illustrated, followed by the original passage reordering method. Then the STG method is presented from the time-clocking perspective, with the passage reordering according to regulated phases. Thirdly the implicit integration for the STG equation system is explained. After that case studies are presented to demonstrate the proposed alterative implementation of the STG method based upon a time-clocking perspective. Results of the harmonic balance method are also presented to contrast the two methods in terms of solution accuracy, time consumption and memory consumption.

2. Methodology

2.1. Space-time gradient method

The Unsteady Reynolds Averaged Navier-Stokes (URANS) equations in a three-dimensional cylindrical coordinate system can be written as

$$\frac{\partial \boldsymbol{Q}}{\partial t}+\frac{\partial(\boldsymbol{F}-\boldsymbol{Q}v_{g,x}-\boldsymbol{V}_x)}{\partial x}+\frac{\partial(\boldsymbol{G}-\boldsymbol{Q}v_{g,\theta}-\boldsymbol{V}_\theta)}{r\partial\theta}+\frac{\partial(\boldsymbol{H}-\boldsymbol{Q}v_{g,r}-\boldsymbol{V}_r)}{r\partial r}-\boldsymbol{S}=\boldsymbol{0} \tag{1}$$

where $\boldsymbol{Q}$ is the vector that represents conservative variables. $\boldsymbol{F}$, $\boldsymbol{G}$ and $\boldsymbol{H}$ are vectors representing convective fluxes; $\boldsymbol{V}_x$, $\boldsymbol{V}_\theta$ and $\boldsymbol{V}_r$ are vectors representing viscous fluxes; $v_{g,x}$, $v_{g,\theta}$ and $v_{g,r}$ represent grid velocity components; $\boldsymbol{S}$ represents the source term vector. The detailed definition of these terms can be found in Ref. 12, thus they are omitted here for simplicity. Eq. (1) can be rewritten as follows to facilitate a simple illustration of the STG method:

$$\frac{\partial \boldsymbol{Q}}{\partial t}+\boldsymbol{R}(\boldsymbol{Q})=\boldsymbol{0} \tag{2}$$

where $\boldsymbol{R}$ is the lumped sum of the spatial derivative and source term. The fundamental idea of the STG method is to solve the flow field variation of corresponding points at different passages of the same blade row at a certain time instant instead of the temporal variation at the same point. For the implementation of the STG method, we mainly focus on the discretization of the temporal derivative term, which is converted to a spatial derivative term as follows.

$$\frac{\partial \boldsymbol{Q}}{\partial t}=\frac{\partial\theta}{\partial t}\cdot\frac{\partial \boldsymbol{Q}}{\partial\theta}=\Omega\frac{\partial \boldsymbol{Q}}{\partial\theta} \tag{3}$$

Substitute Eq. (3) to Eq. (2), we can get the STG equation system

$$\Omega\frac{\partial \boldsymbol{Q}}{\partial\theta}+\boldsymbol{R}(\boldsymbol{Q})=\boldsymbol{0} \tag{4}$$

where Ω denotes the rotational angular velocity of the shaft and θ is the circumferential angular coordinate. Now Eq. (4) becomes a quasi-steady equation system, which means that the circumferential clocking position uniquely determines the instantaneous flow field of a certain passage caused by blade row interaction. To discretize the spatial derivative in a finite difference framework, the key point comes to how to use the flow fields at different passages to construct the difference equation.

Yi and He[10] developed a passage reordering method based on spatial–temporal aliasing to describe the relative clocking position and used it to reorder the passages. Before reordering the passages of a blade row, the relative clocking positions of all passages of one row have to be obtained first. Then all passages of that row can be ordered according to the relative clocking positions in an ascending order. To provide a clear illustration of the calculation of a relative clocking position, we use a hypothetical stage with 8 and 15 passages for the upstream rotor and downstream stator, respectively, as shown in Fig. 1. If we take a certain point in space as the origin, then the corresponding point at each passage has a circumferential coordinate, as shown in Fig. 1(a). The relative clocking position for a downstream stator blade passage Δs is defined as the difference in the tangential coordinate between that passage and the nearest upstream blade passage. Fig. 1(b) presents the reordered passages using this method. All the stator blades are gathered between two adjacent blades of the upstream rotor blade row with a spatial interval of $360°/(N_1N_2)$. N_j is the blade count of the jth row with $j = 1, 2$. It should be noted that the rotor blade passages can be ordered in the same way. Once all the passages are ordered, finite differencing for one blade passage can be accomplished using the current passage and surrounding passages.

2.2. A time-clocking perspective of STG method

For unsteady flows due to blade row interaction, it is well known that the unsteady flows of different passages of the same row have the same magnitude but different phases. The phase difference between adjacent blade passage is called inter blade phase angle and is fixed for any two adjacent passages. With this perception, the unsteady flows of different passages of the same row at a certain time instant can be mapped to the unsteady flows of the same passage at different time instants. This map can be achieved either through time instants or phases of flow fields of different passages, as the time instant and phase have one to one correspondence.

Without loss of generality, assume we have a stage with the first and second rows having blade counts of N_1 and N_2. Fig. 2(a) shows the passages of the first blade row. Assume that the unsteady disturbance from the second row goes in the positive θ direction, the phase φ of the flow field in the ith passage relative to the first passage is given by

$$\varphi_i=(i-1)\frac{N_2}{N_1}\times 360° \tag{5}$$

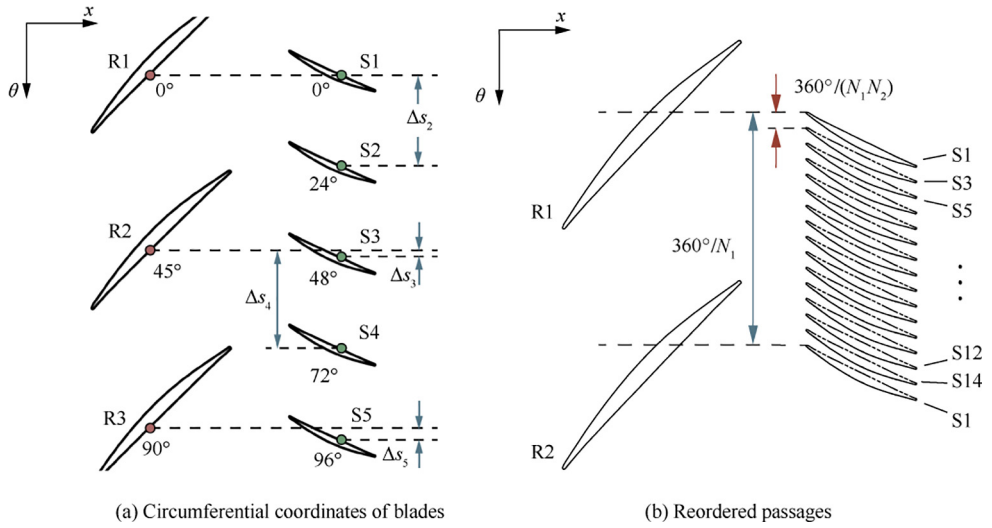

Fig. 1 Original and reordered stator passages of a hypothetical stage using passage reordering method based upon relative space-clocking positions.

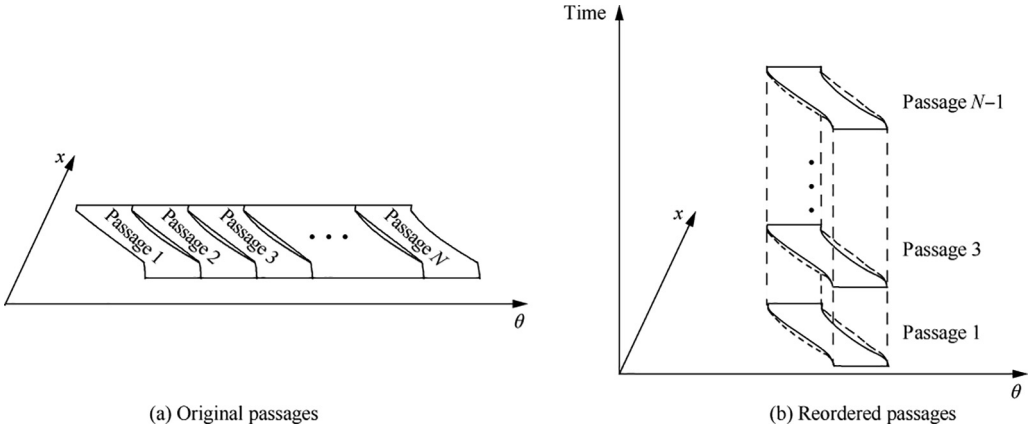

Fig. 2 Passage reordering according to phases of unsteady flows.

where i ranges from 1 to N_1. The phase angle is called a raw phase and its value can be more than 360°. That means the flow fields of different passages span over one period of unsteadiness. Due to the temporal periodicity of the flow fields, we can regulate the raw phases so that they are brought to the range of [0°,360°). The regulated phases can be achieved by simply adding or subtracting multiple of 360° to the raw phases. Passage reordering can be achieved by sorting the regulated phases of all passages in an ascending order. Fig. 2(b) shows the reordered passages. It is worth pointing out the passage reordering based upon the phases provides the same results as that based upon relative clocking positions.

Apart from the time/phase-clocking based passage reordering, we also want to use flow fields at the reordered passages to approximate the original time derivative directly using a finite difference scheme without resorting to a spatial derivative. To do this, the key is to find the proper time step for the finite differencing. The time step is calculated by

$$\Delta t = \frac{\Delta\varphi}{\omega}$$

where ω is angular frequency of unsteadiness and is also the blade passing angular frequency; $\Delta\varphi$ is the phase difference between two adjacent regulated phases. Then the form of the STG equation system from the time-clocking perspective can be written as

$$\frac{\partial \boldsymbol{Q}}{\partial t} + \boldsymbol{R}(\boldsymbol{Q}) = \boldsymbol{0} \tag{6}$$

It is not difficult to find out that the Eq. (6) is the same as the governing equations based upon the perspective of relative clocking position as shown by Eq. (2).

From the time-clocking perspective, one can view the STG method in such a way: the flow fields at different time instants of the same blade passage are solved but are stored at different blade passages of the same row. One can also choose a spectral method to discretize the time derivative. Different from the harmonic balance method, the choice of time instants has restriction: the time instants must correspond to phases/clocking positions of flow fields of different blade passages. The advantage of the STG over the harmonic balance method lies

in the interface treatment: the sliding plane method can be used directly.

2.3. High order difference scheme for STG method

Inheriting the implementation of the DTS method, the discretization of the time derivative can simply use a second order backward difference scheme, which has been demonstrated that the STG method can have the same convergence characteristic as the frozen rotor method. Different from the DTS method, for which a time step can be specified with a certain freedom, the time step for the STG method is related to the blade counts of a stage and cannot be specified at will. If the blade count of a blade row is small, then the time step can be too large to deliver acceptable solution accuracy when the second order backward differencing is used. Under these circumstances, there is a need to use a higher order scheme to ensure a reliable solution if one does not want to resort to more time instants. However, a high order scheme quite often gives a poor convergence or even causes solution instability. Fig. 3 shows the convergence histories of the continuity equation using the STG method with the second (STG 2) and ninth order difference schemes (STG 9), respectively, where R_ρ represents the residual of the density. The ninth order scheme cannot get a fully converged solution when the pseudo-time derivative is discretized explicitly.

Huang et al.[13] proposed the Lower-Upper Symmetric Gauss–Seidel/Gauss–Seidel (LU-SGS/GS) method for an implicit solution of the HB equation system. The method can offer fast and tight convergence characteristic for turbomachinery blade row interaction unsteady flows. This method can also be adapted for an implicit integration of the STG equation system to ensure a stable solution when a high order difference scheme is used. Adding a pseudo time derivative to Eq. (6), the STG equation system can be written in the following form

$$\frac{\partial \boldsymbol{Q}}{\partial \tau} + \frac{\partial \boldsymbol{Q}}{\partial t} + \boldsymbol{R}(\boldsymbol{Q}) = \boldsymbol{0} \tag{7}$$

In this study, finite difference schemes are used to discretize the physical time derivative. For a nth order difference scheme, we have

$$\frac{\partial \boldsymbol{Q}^i}{\partial t} = \frac{1}{\Delta t}\sum_{k=k_\mathrm{l}}^{k_\mathrm{u}} \beta_k \boldsymbol{Q}^{i+k} \tag{8}$$

where i is the index of the reordered passages, and it ranges from 1 to N_p. N_p is the number of passages for a row in the computational domain. k_l and k_u satisfy $k_\mathrm{u} - k_\mathrm{l} = n$. A second order backward difference scheme and ninth order mixed difference scheme are implemented in the STG solver. For the second order scheme, $k_\mathrm{l} = -2$ and $k_\mathrm{u} = 0$, the difference coefficients of β_k are given by

$$\beta_{-2} = \frac{1}{2}, \beta_{-1} = -2, \beta_0 = \frac{3}{2} \tag{9}$$

For a ninth order mixed difference scheme, $k_\mathrm{l} = -5$ and $k_\mathrm{u} = 4$, we have the difference coefficients of β_k as

$$\begin{aligned} &\beta_{-5} = -\frac{1}{630}, \beta_{-4} = \frac{1}{56}, \beta_{-3} = -\frac{2}{21}, \beta_{-2} = \frac{1}{3}, \\ &\beta_{-1} = -1, \beta_0 = \frac{1}{5}, \beta_1 = \frac{2}{3}, \beta_2 = -\frac{1}{7}, \beta_3 = \frac{1}{42}, \\ &\beta_4 = -\frac{1}{504} \end{aligned} \tag{10}$$

The stabilities of these two schemes have been investigated with matrix analyses by Zhang and Wang.[14] It is worth pointing out that the ninth order scheme here utilizes stencils on two sides, which is impossible for the DTS method. For cases where the number of passages is more than 10, the high order difference scheme has better locality for the time derivative calculation, thus it has lower time cost compared with the harmonic balance method. Furthermore, the difference scheme is even more stable than the harmonic balance method.

The STG equation system after the discretization of the time derivative can be written as follows

$$\begin{cases} \frac{\partial \boldsymbol{Q}^1}{\partial \tau} + \frac{1}{\Delta t}\sum_{k=k_\mathrm{l}}^{k_\mathrm{u}} \beta_k \boldsymbol{Q}^{1+k} + \boldsymbol{R}(\boldsymbol{Q}^1) = \boldsymbol{0} \\ \frac{\partial \boldsymbol{Q}^2}{\partial \tau} + \frac{1}{\Delta t}\sum_{k=k_\mathrm{l}}^{k_\mathrm{u}} \beta_k \boldsymbol{Q}^{2+k} + \boldsymbol{R}(\boldsymbol{Q}^2) = \boldsymbol{0} \\ \vdots \\ \frac{\partial \boldsymbol{Q}^{N_\mathrm{p}}}{\partial \tau} + \frac{1}{\Delta t}\sum_{k=k_\mathrm{l}}^{k_\mathrm{u}} \beta_k \boldsymbol{Q}^{N_\mathrm{p}+k} + \boldsymbol{R}(\boldsymbol{Q}^{N_\mathrm{p}}) = \boldsymbol{0} \end{cases} \tag{11}$$

It should be noted that $\boldsymbol{Q}^{1+k} = \boldsymbol{Q}^{N_\mathrm{p}+1+k}$. The solutions at all passages form the vector $\boldsymbol{Q}^* = \left[\boldsymbol{Q}^1, \boldsymbol{Q}^2, \cdots, \boldsymbol{Q}^{N_\mathrm{p}}\right]^\mathrm{T}$. And then the equations above can be organized into the following matrix form

$$\frac{\partial \boldsymbol{Q}^*}{\partial \tau} + \boldsymbol{M}\boldsymbol{Q}^* + \boldsymbol{R}(\boldsymbol{Q}^*) = \boldsymbol{0} \tag{12}$$

where the matrix $\boldsymbol{M}$ is given by

$$\boldsymbol{M} = \frac{1}{\Delta t}\begin{pmatrix} \beta_0 & \cdots & \beta_{k_\mathrm{u}-3} & \beta_{k_\mathrm{u}-2} & \beta_{k_\mathrm{u}-1} & \beta_{k_\mathrm{u}} & 0 & 0 & \cdots & 0 & 0 & 0 & 0 & \beta_{k_\mathrm{l}} & \beta_{k_\mathrm{l}+1} & \cdots & \beta_{-1} \\ \beta_{-1} & \cdots & \beta_{k_\mathrm{u}-4} & \beta_{k_\mathrm{u}-3} & \beta_{k_\mathrm{u}-2} & \beta_{k_\mathrm{u}-1} & \beta_{k_\mathrm{u}} & 0 & \cdots & 0 & 0 & 0 & 0 & 0 & \beta_{k_\mathrm{l}} & \cdots & \beta_{-2} \\ \vdots & & \vdots & \vdots & \vdots & \vdots & \vdots & \vdots & & \vdots & \vdots & \vdots & \vdots & \vdots & \vdots & & \vdots \\ \beta_2 & \cdots & \beta_{k_\mathrm{u}-1} & \beta_{k_\mathrm{u}} & 0 & 0 & 0 & 0 & \cdots & 0 & 0 & \beta_{k_\mathrm{l}} & \beta_{k_\mathrm{l}+1} & \beta_{k_\mathrm{l}+2} & \beta_{k_\mathrm{l}+3} & \cdots & \beta_1 \\ \beta_1 & \cdots & \beta_{k_\mathrm{u}} & 0 & 0 & 0 & 0 & 0 & \cdots & 0 & \beta_{k_\mathrm{l}} & \beta_{k_\mathrm{l}+1} & \beta_{k_\mathrm{l}+2} & \beta_{k_\mathrm{l}+3} & \beta_{k_\mathrm{l}+4} & \cdots & \beta_0 \end{pmatrix} \tag{13}$$

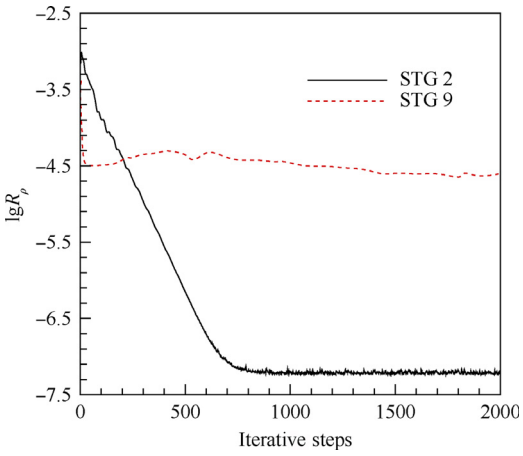

Fig. 3 Convergence histories of continuity equation from STG methods with two differencing schemes.

$\boldsymbol{M}$ is a sparse and circulant symmetric square matrix with the dimension of N_p, which makes it less time consuming to be calculated when compared with the corresponding term of the HB method. The time derivative is calculated based upon Eq. (8) instead of Eq. (13) from an implementation perspective.

Omitting the superscript for simplicity, an implicit time integration of Eq. (12) is given by

$$\frac{\Delta \boldsymbol{Q}}{\Delta \tau} + \boldsymbol{M}\boldsymbol{Q}^{n+1} + \boldsymbol{R}(\boldsymbol{Q}^{n+1}) = \boldsymbol{0} \tag{14}$$

A first-order Taylor's expansion is used to approximate the lumped sum residual

$$\boldsymbol{R}(\boldsymbol{Q}^{n+1}) \approx \boldsymbol{R}(\boldsymbol{Q}^{n}) + \frac{\partial \boldsymbol{R}}{\partial \boldsymbol{Q}}\Delta \boldsymbol{Q} = \boldsymbol{R}(\boldsymbol{Q}^{n}) + \boldsymbol{A}\Delta \boldsymbol{Q} \tag{15}$$

Eq. (14) can be rewritten as the following form

$$\begin{aligned}(\boldsymbol{I} + \Delta\tau\boldsymbol{M} + \Delta\tau\boldsymbol{A})\Delta\boldsymbol{Q} &= \Delta\tau(-\boldsymbol{M}\boldsymbol{Q}^{n} - \boldsymbol{R}(\boldsymbol{Q}^{n})) \\ &= \Delta\tau\,\widehat{\boldsymbol{R}}(\boldsymbol{Q}^{n})\end{aligned} \tag{16}$$

The matrix of $\boldsymbol{I} + \Delta\tau\boldsymbol{M} + \Delta\tau\boldsymbol{A}$ has to be inverted when solving this equation directly, which is complicated because $\boldsymbol{I} + \Delta\tau\boldsymbol{M} + \Delta\tau\boldsymbol{A}$ contains the flow field information at all control volumes in all passages. To reduce the complexity, the LU-SGS/GS method is employed to solve the equation above.

First to factorize $\boldsymbol{I} + \Delta\tau\boldsymbol{M} + \Delta\tau\boldsymbol{A}$, we have

$$\boldsymbol{I} + \Delta\tau\boldsymbol{M} + \Delta\tau\boldsymbol{A} = (\boldsymbol{I} + \Delta\tau\boldsymbol{A})(\boldsymbol{I} + \Delta\tau\boldsymbol{M}) - (\Delta\tau)^2\boldsymbol{M}\boldsymbol{A} \tag{17}$$

Ignore the last term on the right hand side, substitute the above equation to Eq. (16) as follows.

$$(\boldsymbol{I} + \Delta\tau\boldsymbol{A})(\boldsymbol{I} + \Delta\tau\boldsymbol{M})\Delta\boldsymbol{Q} \approx \Delta\tau\,\widehat{\boldsymbol{R}}(\boldsymbol{Q}^{n}) \tag{18}$$

The equation above can be solved in two steps:

$$\begin{cases}(\boldsymbol{I} + \Delta\tau\boldsymbol{A})\Delta\boldsymbol{Q}^{1/2} = \Delta\tau\,\widehat{\boldsymbol{R}}(\boldsymbol{Q}^{n}) \\ (\boldsymbol{I} + \Delta\tau\boldsymbol{M})\Delta\boldsymbol{Q} = \Delta\boldsymbol{Q}^{1/2}\end{cases} \tag{19}$$

The first equation is solved by the LU-SGS method. The solution of the second equation can be solved directly due to the sparsity of the matrix $\boldsymbol{M}$ in the case of a small number of passages in the computational domain. To ensure less time and memory consumption in any case, and to reduce the complexity of coding, the second equation can be solved using a Jacobi iteration as

$$\Delta\boldsymbol{Q}^{n} = \Delta\boldsymbol{Q}^{1/2} - \Delta\tau\boldsymbol{M}\Delta\boldsymbol{Q}^{n-1} \tag{20}$$

For $m = 1$, let $\Delta\boldsymbol{Q}^{0} = \Delta\boldsymbol{Q}^{1/2}$. Eq. (20) can be arranged as

$$\Delta\boldsymbol{Q}^{1} = (\boldsymbol{I} - \Delta\tau\boldsymbol{M})\Delta\boldsymbol{Q}^{1/2} \tag{21}$$

Then this equation can be solved by one-step Gauss-Seidel (GS) iteration

$$-\boldsymbol{L}\Delta\boldsymbol{Q}^{1} = \boldsymbol{U}\Delta\boldsymbol{Q}^{1/2} \tag{22}$$

where $-\Delta\tau\boldsymbol{M} = \boldsymbol{L} + \boldsymbol{U}$ with $\boldsymbol{L}$ being the lower triangular matrix and $\boldsymbol{U}$ being the strictly upper triangular matrix.

2.4. Baseline flow solver

The studies in this paper are based on the in-house flow solver-TurboXD, which solves the three-dimensional URANS equations in a cylindrical coordinate system for turbomachinery. The URANS equations are closed using the Spalart-Allmaras turbulence model with helicity correction.[15] Solution of the above equation is calculated by using a cell-centered finite volume approach. Spatial discretization employs the Jameson-Schmidt-Turkel (JST) scheme[16] with scaled numerical dissipation to avoid excessive numerical dissipation. A hybrid five-stage Runge-Kutta method[16] is implemented for the time integration in pseudo time. The LU-SGS method[17] is invoked as a residual smoother to achieve an efficient simulation. To speed up the solution convergence, a V type multigrid and local time step are also utilized in the code.

The implementation of the STG method is based on a pure shared memory mode (pure open multi-processing mode), which achieves parallel solutions of each passage for the STG method. The Message Passing Interface (MPI) is used for parallel solutions of each blade row.

3. Validation and verification of STG solver

In this section, the original NASA Stage 35 and a variant with reduced blade counts are used to verify the proposed alterative implementation of the STG method with the second and ninth order difference schemes. The results of the HB method will be presented as the benchmark.

3.1. Transonic compressor stage

The transonic compressor stage—NASA Stage 35 is used as the test case to do the validation and verification of the alterative implementation of the STG method and the STG method with a ninth order difference scheme. This stage has a low aspect ratio and represents the inlet stage of a multi-stage compressor. It has a stage peak isentropic efficiency of 87.2% at its design speed. The corresponding mass flow rate and stage pressure ratio is 20.8 kg/s and 1.82, respectively. The measured stage stall margin is 21.8% at design speed. The design specifications and geometry data can be found in the report by Reid and Moore.[18]

An H-type mesh topology is used to mesh the blade passages. For each blade passage, there are 73 grid points in the

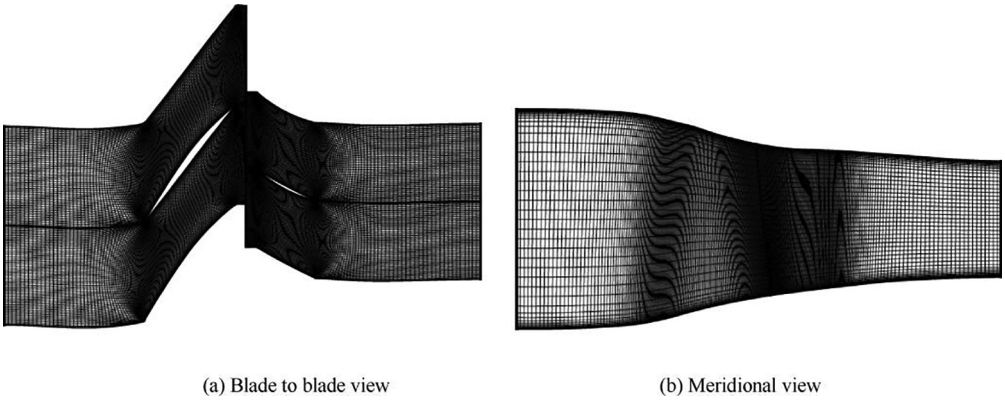

(a) Blade to blade view (b) Meridional view

Fig. 4 Blade to blade view and meridional view of computational grid for NASA Stage 35 compressor.

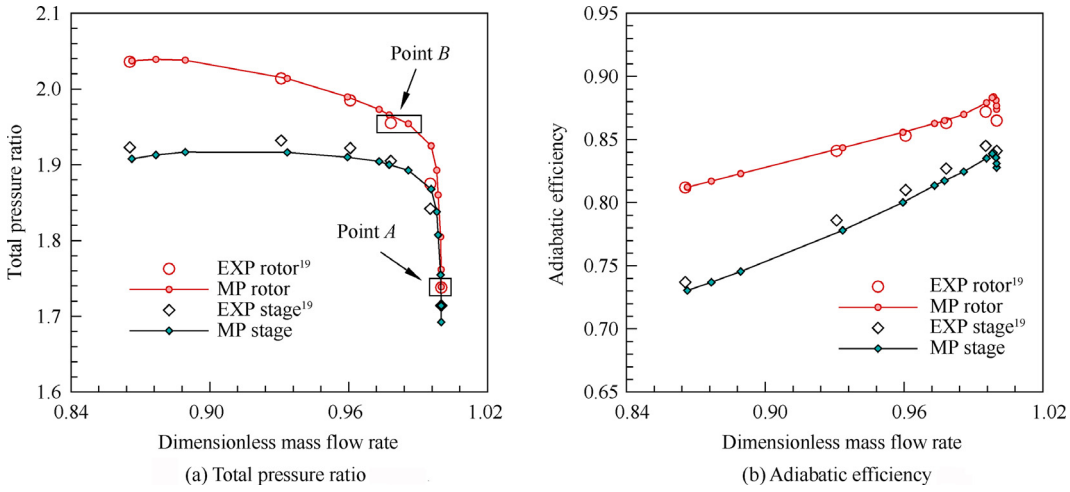

(a) Total pressure ratio (b) Adiabatic efficiency

Fig. 5 Rotor and stage performance maps.

radial direction, 57 grid points in the circumferential direction, and 185 grid points in the axial direction. The total number of grid points is about 0.77 million for each passage. Fig. 4 shows the blade to blade view (at 50% blade span) and meridional view of the computational grid.

The rotor and stage performance maps predicted by the MP approach are shown in Fig. 5. The mass flow rates are normalized by choke mass flow rates. The calculated choke mass flow rate and measured one are 20.75 kg/s and 21.1 kg/s, respectively. The calculated overall performance is in good agreement with the measurement data. In the following, two operating points, namely Point *A* and Point *B*, as marked in Fig. 5(a), are considered for validating the STG solver. The same rotor pressure ratio is used as the reference for selecting the corresponding operating points from numerical and experimental data. Detailed flow measurements were conducted at the two operating points and reported by NASA in 1978.[19] These measured data are available in terms of radial profiles of total pressure, total temperature, and adiabatic efficiency.

3.2. Results and discussion

To verify the proposed numerical methods and their proper implementation in the STG solver, the results from an existing HB solver will be used as the references. It should be noted that the HB solver has been extensively validated by Huang et al.[13] The treatment at the rotor–stator interface of the HB method was reported in Ref. 20. The HB method uses a domain of one blade passage for each blade row. Four and eight harmonics are used for the rotor and stator domains, respectively, in a harmonic balance analysis. As the stage has 36 rotor blades and 46 stator blades, the computational domain for the STG method is half an annulus. Part of the reordered passage indices and the corresponding regulated phases, obtained by the time/phase-clocking based passage

Table 1 Reordered passage indices and regulated phases for NASA Stage 35.

Reordered/ original rotor passage index	Regulated phase for rotor (°)	Reordered/ original stator passage index	Regulated phase for stator (°)
1/1	0	1/1	0
2/8	20	2/10	15.65
3/15	40	3/19	31.30
4/4	60	4/5	46.96
5/11	80	5/14	62.61

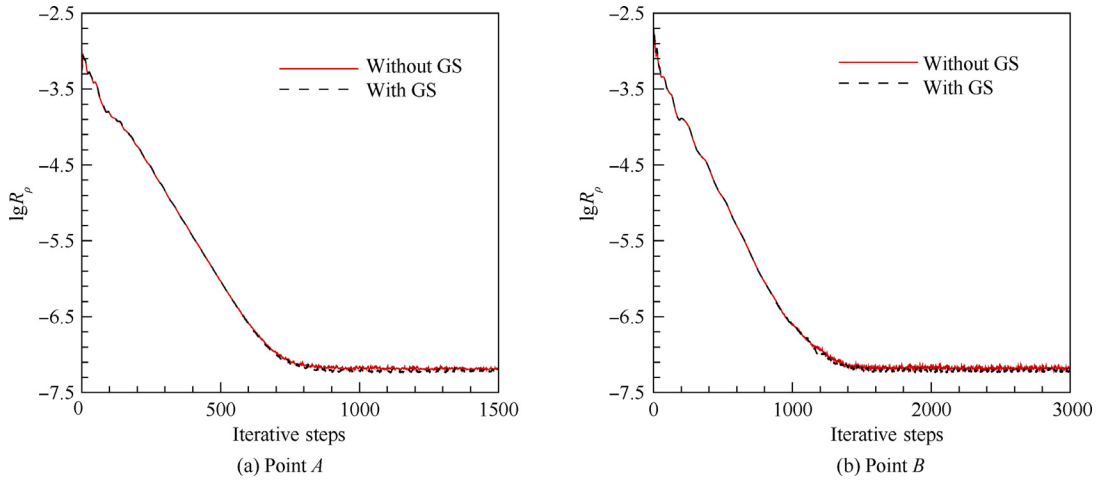

Fig. 6 Convergence histories of continuity equation using STG 2 with/without GS method.

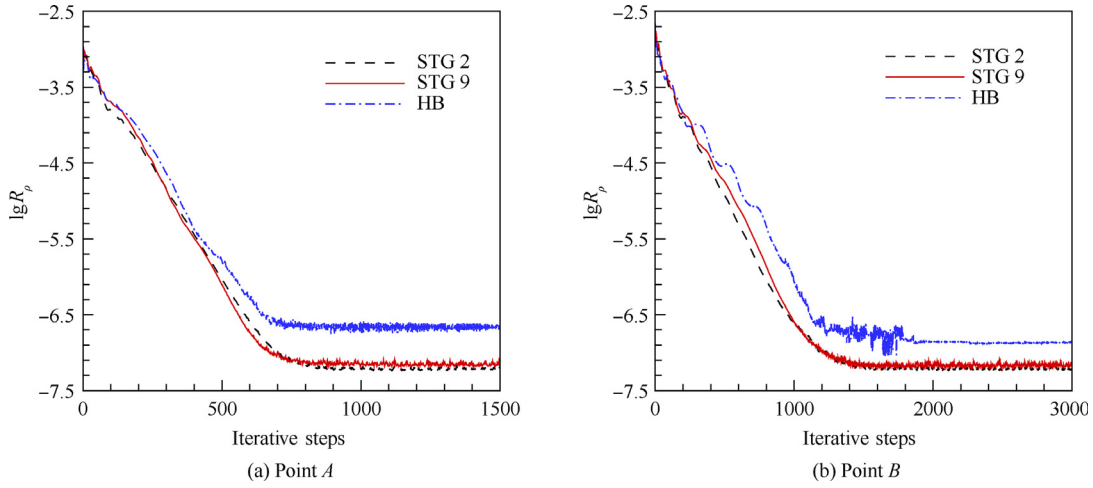

Fig. 7 Convergence histories of continuity equation using STG methods and HB method.

Table 2 Overall performance metrics by HB method at Point A and Point B.

Operating point	Mass flow rate (kg/s)	π*(rotor)	η(rotor)	π* (stage)	η(stage)
Point A	20.746	1.739	0.870	1.711	0.842
Point B	19.396	1.955	0.837	1.887	0.788

reordering, are shown in Table 1. The original passages are ordered in an ascending order according to the regulated phases. A series of analyses have been performed using the developed STG solver: analyses using a second order difference scheme (STG 2) and a ninth order difference scheme (STG 9) for the time derivative.

Fig. 6 shows the convergence histories of the continuity equation from analyses using the STG method with a second order backward difference (STG 2) with/without the GS method (the LU-SGS method is always applied to solve the first equation of Eq. (19)). The LU-SGS/GS method only improves the convergence slightly. However, as shown in Fig. 3 and Fig. 7, the LU-SGS/GS can improve the convergence of STG 9 considerably. The convergence histories of STG 2 and STG 9 with an implicit solution are almost the same. Furthermore, compared with the HB solution, the STG solutions have tighter convergence as indicated by the smaller final residuals in Fig. 7. The benchmark HB results are listed in Table 2. Note that π* and η represent total pressure ratio and adiabatic efficiency, respectively. And the relative differences between other calculations and the benchmark HB results are visualized in Fig. 8.

At Point A, the results obtained from the three unsteady analyses are very close to each other and also close to those from a steady MP analysis. The discrepancies between steady and unsteady analyses at Point B are large due to

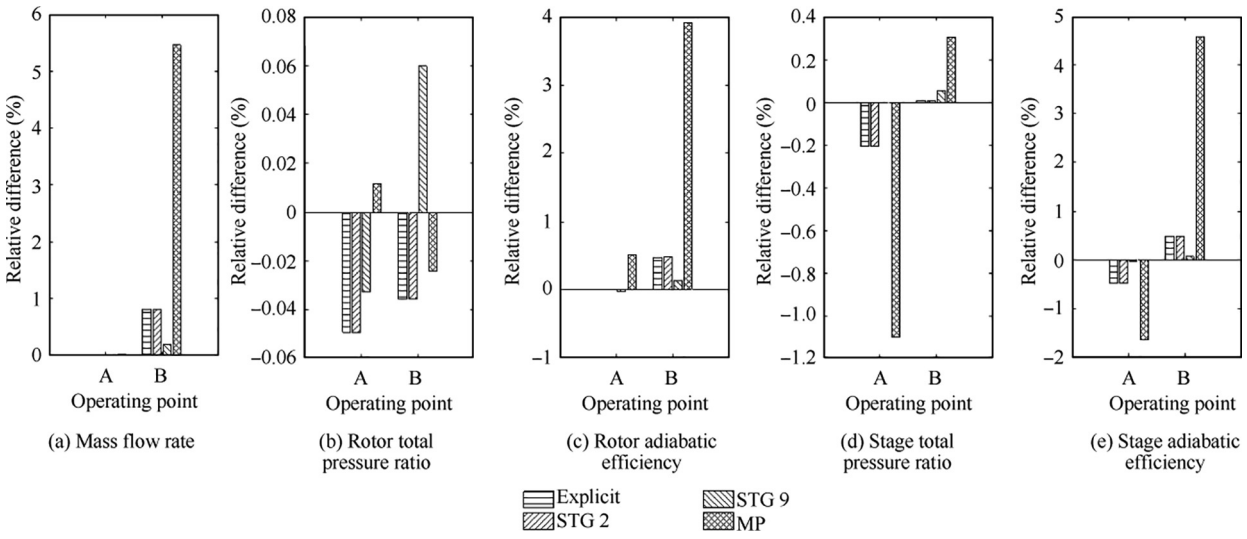

Fig. 8 Relative differences of overall performance metrics at different operating points with respect to benchmark HB results.

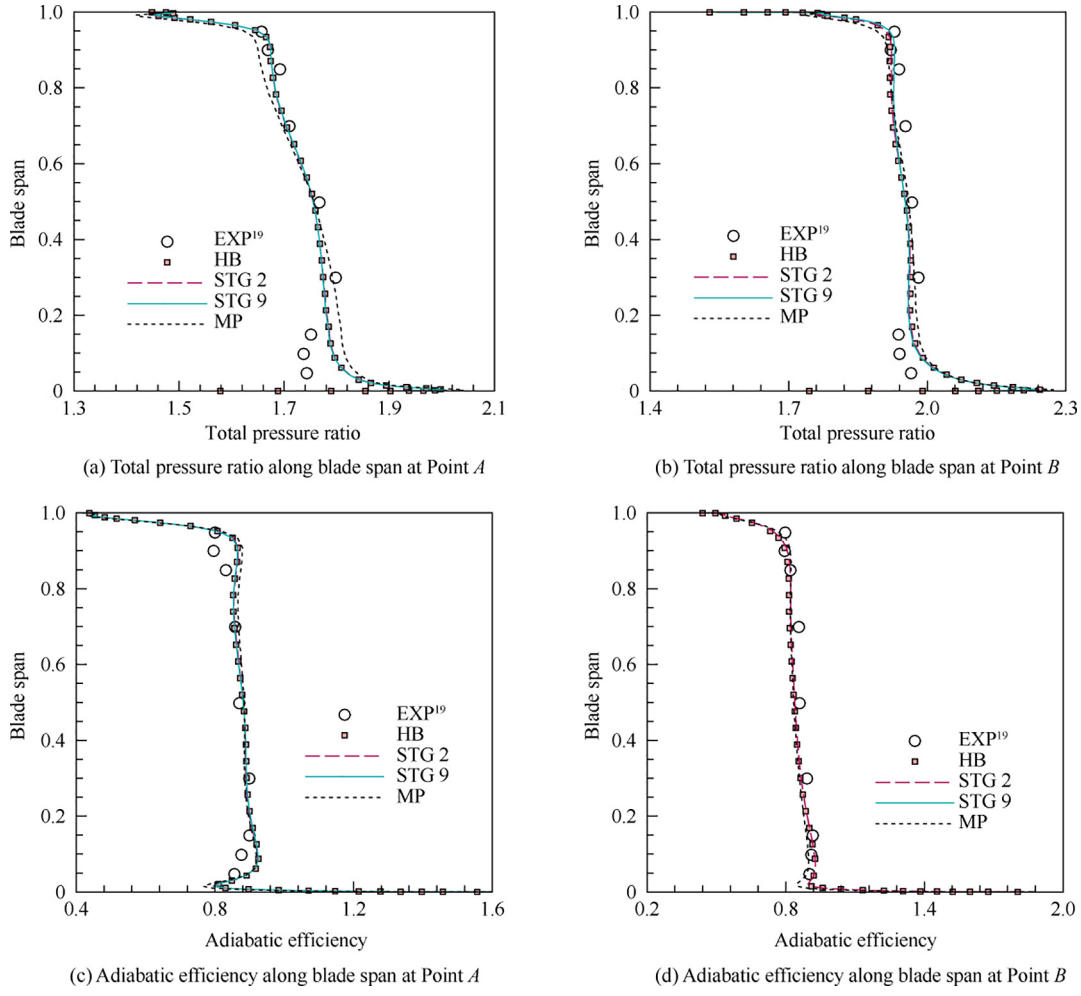

Fig. 9 Circumferential mass averaged radial profiles at rotor exit.

the unsteady flow features caused by the strong flow separation on the blade suction side to be presented later. The overall performances predicted by the STG method using the second order scheme is independent of the use of the GS method as expected. The deviation of STG 2 and STG 9 results from the HB results is not significant. The STG 9 results are generally closer to the benchmark HB results than those of STG 2.

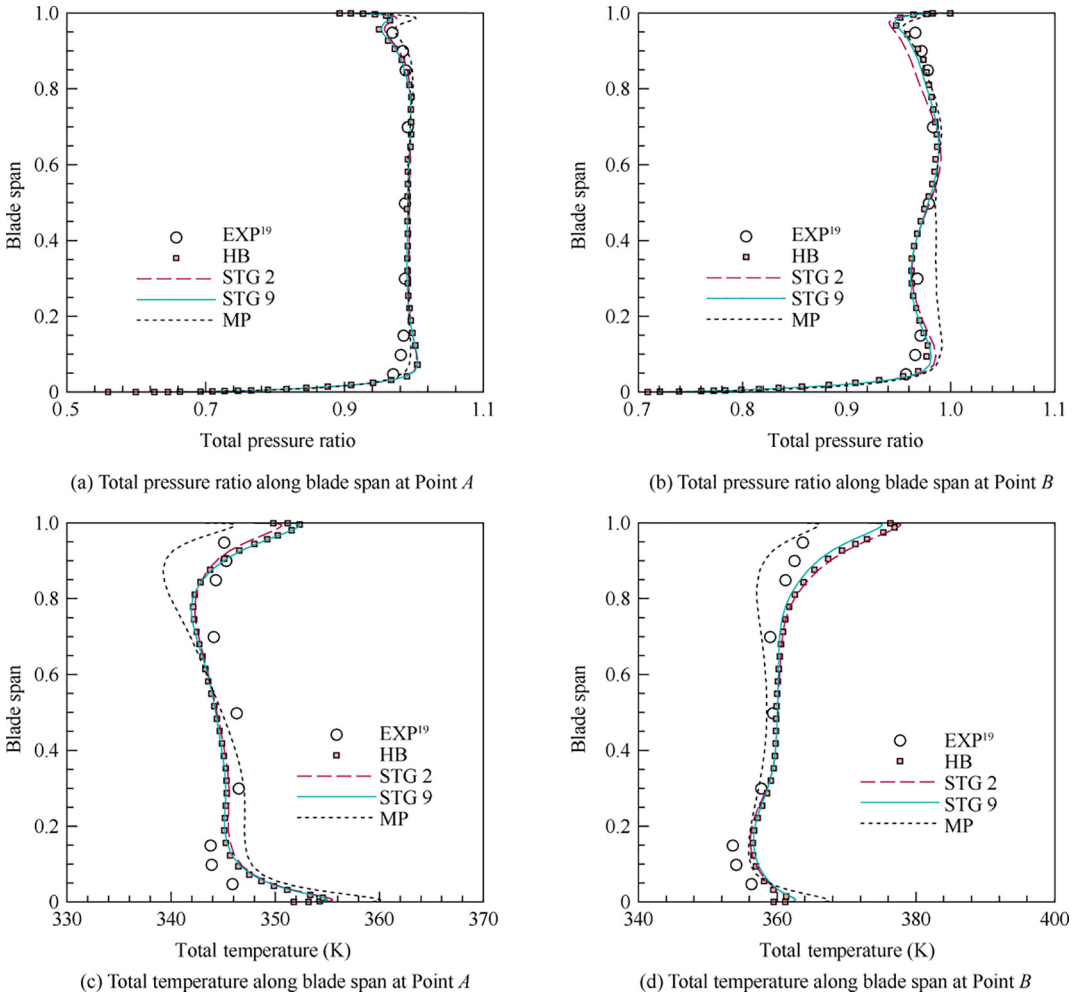

Fig. 10 Circumferential mass averaged radial profiles at stator exit.

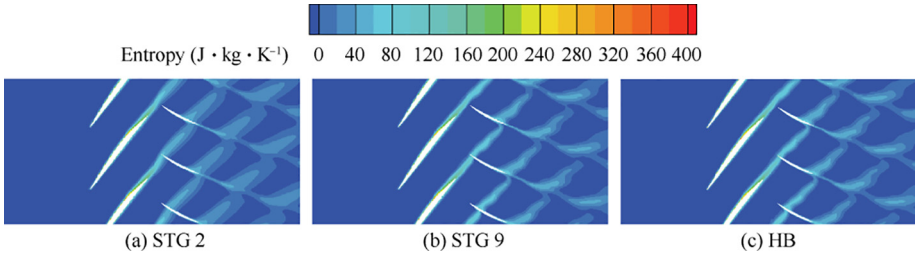

Fig. 11 Entropy contours of 50% blade span at Point *A*.

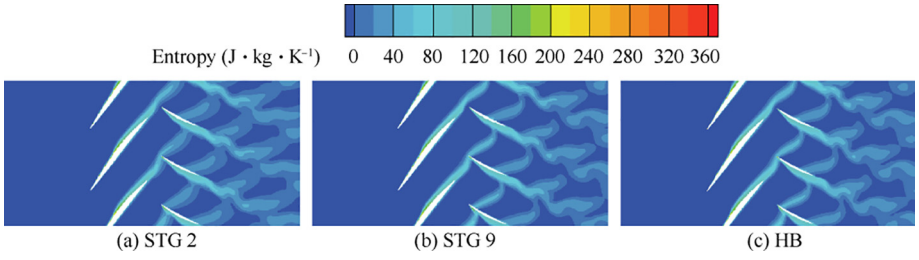

Fig. 12 Entropy contours of 50% blade span at Point *B*.

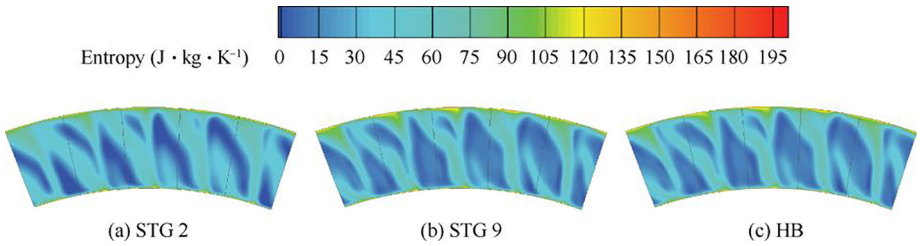

Fig. 13 Entropy contours at stator exit station at Point *A*.

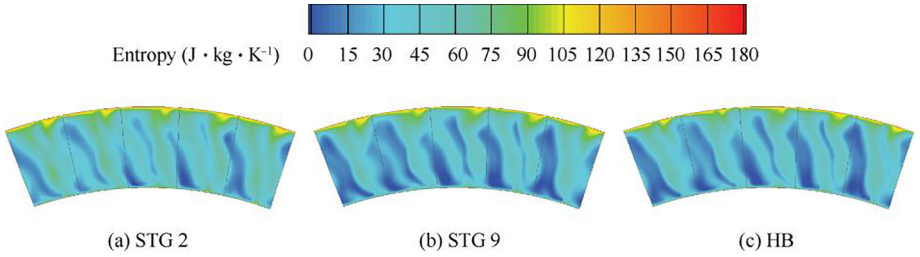

Fig. 14 Entropy contours at stator exit station at Point *B*.

Fig. 9 and Fig. 10 compare calculated circumferential mass averaged radial profiles at the rotor and stator exit at Point *A* and Point *B* with experimental data from the experiment numbers of 4004 and 3977, respectively.[19] The results of STG 2 without the GS method are not presented due to the solution independent of the use of the GS method. Results predicted by the MP approach are also provided here to show the solution improvement from a steady analysis to an unsteady analysis.

Radial profiles at the rotor exit are shown in Fig. 9. Here all three unsteady solution methods give remarkably similar results that agree very well with the experimental data. At the stator exit, the radial profiles with these three unsteady solution methods have some small differences as shown in Fig. 10. STG 9 and HB predict the similar results that both show quantitatively good agreement with experimental data in general. Though the STG 2 results give some small deviations in predicting the solution at the high blade span, they still show a solution improvement compared to the MP results.

Fig. 11 and Fig. 12 show the instantaneous entropy at 50% blade span at Point *A* and Point *B*, respectively. Entropy from the upstream blade row enters the downstream blade row across the rotor–stator interface. It can be seen that there is little difference in the entropy contours between STG 9 and HB. While the rotor wakes in the stator domain as predicted by STG 2 are smeared, which is caused by the higher dissipation of the second order scheme.

To further compare the three methods, entropy contours at the stator exit are presented in Fig. 13 and Fig. 14. The solution predicted by STG 9 is almost non-distinguishable from the solution by HB, while STG 2 gives some marked discrepancies. At Point *A*, STG 2 predicts the lowest peak entropy. The higher dissipation of the second order scheme smears the highest entropy region. The situation at Point *B* is different

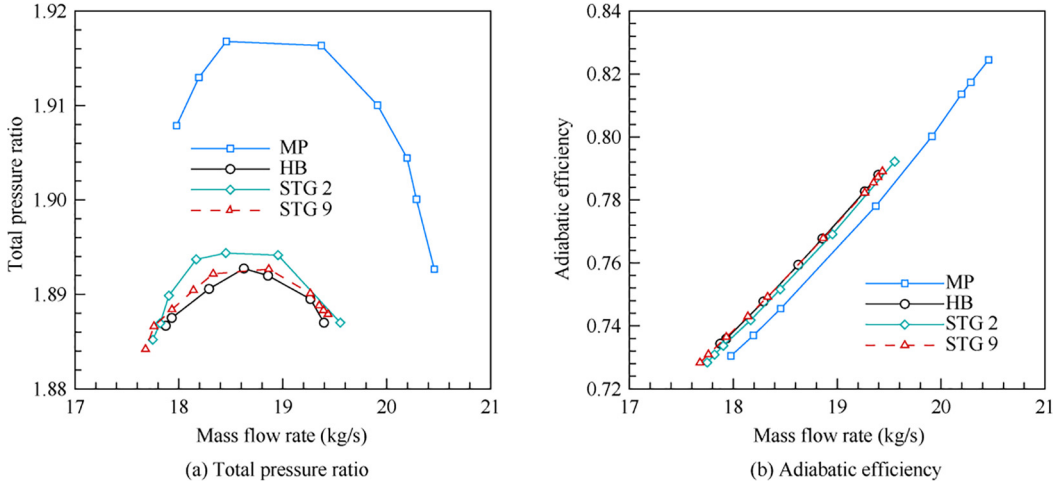

Fig. 15 Stage performance maps at left side of Point *B*.

Table 3 Reordered passage indices and regulated phases for blade-count-reduced NASA Stage 35 variant.

Reordered/ original rotor passage index	Regulated phase for rotor (°)	Reordered/ original stator passage index	Regulated phase for stator (°)
1/1	0	1/1	0
2/4	90	2/5	72
3/3	180	3/4	144
4/2	270	4/3	216
		5/2	288

from that at Point *A*. The entropy by STG 2 is stronger than the other two results as shown in Fig. 14. The numerical dissipation of the second order scheme leads to the smeared wake mixing region at the stator domain as shown in Fig. 12, which causes the stronger entropy.

The effectiveness of the proposed implementation of the STG method has been clearly demonstrated by the above analyses. The ninth order mixed difference scheme can improve the solution accuracy indeed without numerical instability, when the LU-SGS/GS method is used.

To evaluate the stall margin predicted by these three methods, the performance maps at the left side of Point *B* are calculated as shown in Fig. 15. Unsteady analyses give the same trend on the performance map compared with the steady analyses: the lower mass flow rate, the lower total pressure ratio, and the higher adiabatic efficiency. The results predicted by STG 9 are closer to those by HB, which is consistent with results presented in the previous sections. The results of the near stall points are obtained by sweeping back pressure in the increment of 100 Pa. The back pressure of the final operating point from each method is different (144.8 kPa for STG 2, 144.7 kPa for STG 9 and 144 kPa for HB). According to the definition of stall margin, we have:

$$\mathrm{SM} = \left(\frac{\pi_s^*}{\pi_d^*} \cdot \frac{G_d}{G_s} - 1\right) \times 100\% \tag{23}$$

where G denotes the mass flow rate, the subscripts "d" and "s" refer to the design point and the near stall point, respectively. And $G_d = 20.188$ kg/s, and $\pi_d^* = 1.82$. The stall margins of STG 2, STG 9 and HB are 17.81%, 18.22% and 17.08%, respectively. This indicates that the STG method has a better solution stability at the near stall region, which may be attributed to the higher stability of the difference scheme. It should be noted that the stability of HB depends on the number of harmonics being used. The inclusion of higher harmonics reduces the solution stability.

3.3. Further demonstration of the ninth order difference scheme

To further demonstrate the great accuracy improvement of the ninth order difference scheme for the STG method, the number of stator vanes of NASA Stage 35 is adjusted to 45, then there are only 4 and 5 passages in the computational domain for the rotor and stator, respectively, for the STG method. This is quite an extreme case because the numbers of rotor blades and stator vanes are generally set to be mutually prime in modern turbomachinery designs to avoid resonance. Consequently, the required number of passages for a row in the domain is much bigger in most cases when the STG method is used, which ensures a good solution accuracy for CFD simulation due to a small time step.

The reordered passage indices and regulated phases are listed in Table 3. Referring to Table 1, it can be derived that the time step of the blade-count-reduced NASA Stage 35 variant is about 4.5 times larger than that of the original geometry.

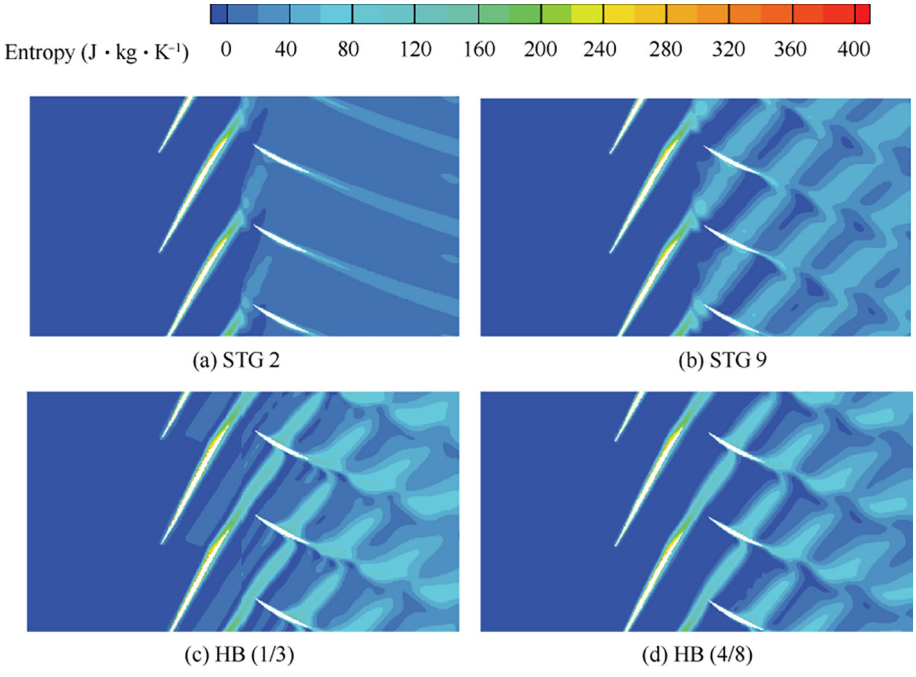

Fig. 16 Entropy contours at 90% blade span.

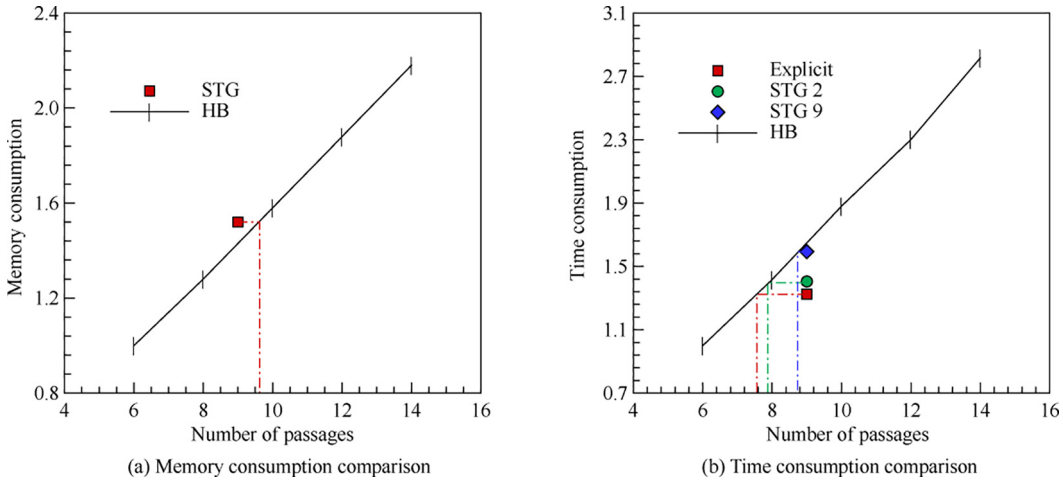

(a) Memory consumption comparison (b) Time consumption comparison

Fig. 17 Comparisons of memory and time consumption.

Thus, a higher order difference scheme for the time discretization is vitally important for good solution accuracy.

One operating point is calculated by the STG method and the HB method, respectively. For the HB method, two configurations of harmonics (1/3 and 4/8 for the rotor/stator domain) are adopted for the unsteady analyses. Thus, 10 and 26 equivalent passages are solved by HB (1/3) and HB (4/8), respectively. Shown in Fig. 16 are the instantaneous entropy contours of 90% blade span. For STG 2, the wake dissipation is dramatic due to the numerical dissipation caused by the second order difference scheme. HB (1/3) solves the flow field for an equivalently similar number of passages. Its entropy contours show some discontinuities along the blade row interface which is caused by the insufficient number of harmonics being retained in the analysis (Gibbs phenomenon). Entropy contours by STG 9 have some spikes along the blade row interface compared with that by HB (4/8), but the overall agreement between STG 9 and HB (4/8) is much better than that of STG 2.

3.4. Memory and time consumption comparison

The blade-count-reduced NASA Stage 35 variant is used to do the comparison of memory and time consumption. The time and memory consumption by one method largely depends on the number of passages (or equivalent passages for the HB method). There are nine passages in the computational domain for the STG methods. The number of equivalent passages for the HB method depends on the number of harmonics being retained in an analysis. The HB method with 2–6 harmonics (6–14 equivalent passages) in total is used to contrast with the STG method. The relationships between the number of passages and the memory/time consumption are given in Fig. 17 (solution of the HB method with 2 harmonics as the reference).

The applications of the implicit solution method and the high order scheme for the STG equation system does not incur additional memory consumption. The memory consumption of the STG method is slightly larger than the HB method when solving for the same numbers of passages. The time consumption of STG 2 is 1.06 times that of the corresponding explicit (STG 2 without the GS method) solution, and STG 9 takes 1.12 times the cost of STG 2. The time consumption of the STG method is less than the HB method when solving for the same number of passages.

4. Conclusions

An alternative implementation of the STG method has been proposed from a time-clocking perspective. The unsteady flow fields from different passages of the same blade row are mapped to unsteady flow fields of the same blade passage at different time instants. The alternative implementation uses the time/phase-clocking based passage reordering. The discretization of the time derivative is performed in time directly instead of replacing the time derivative with a spatial derivative. A ninth order difference scheme has been investigated for discretizing the time derivative to improve the solution accuracy. To guarantee a stable solution for the high order scheme, the LU-SGS/GS method has been applied.

Analyses show that the time-clocking based passage reordering can provide the same passage ordering results as expected. The improvement of the simulation accuracy of the ninth order difference scheme is significant for cases with fewer passages in a domain. All the results are validated by the experimental data as a physical benchmark or solutions predicted by the HB method as a numerical benchmark. The comparison of the predicted stall margin of NASA Stage 35 shows that the STG method has a better solution stability than the HB method at the near stall region.

The employment of the implicit solution method and the high order difference scheme for the STG method do not cause additional memory consumption. The STG method has a slightly larger memory consumption, but less time consumption compared with the HB method when solving for equivalently same number of passages.

Declaration of Competing Interest

The authors declare that they have no known competing financial interests or personal relationships that could have appeared to influence the work reported in this paper.

Acknowledgements

This study was co-supported by the National Natural Science Foundation of China (No. 51976172) and the National Science and Technology Major Project of China (No. 2017-II-0009-0023).

References

1. Denton JD. The calculation of three-dimensional viscous flow through multistage turbomachines. *J Turbomach* 1992;**114**(1):18–26.
2. Jameson A. Time dependent calculations using multigrid, with applications to unsteady flows past airfoils and wings. Reston: AIAA; 1991. Report No.: AIAA-1991-1596.
3. He L. Fourier methods for turbomachinery applications. *Prog Aerosp Sci* 2010;**46**(8):329–41.
4. Erdos JI, Alzner E, McNally W. Numerical solution of periodic transonic flow through a fan stage. *AIAA J* 1977;**15**(11):1559–68.
5. He L. An Euler solution for unsteady flows around oscillating blades. *J Turbomach* 1990;**112**(4):714–22.
6. Hall KC, Ekici K, Thomas JP, et al. Harmonic balance methods applied to computational fluid dynamics problems. *Int J Comput Fluid Dyn* 2013;**27**(2):52–67.
7. Sicot F, Guédeney T, Dufour G. Time-domain harmonic balance method for aerodynamic and aeroelastic simulations of turbomachinery flows. *Int J Comput Fluid Dyn* 2013;**27**(2):68–78.
8. Sicot F, Dufour G, Gourdain N. A time-domain harmonic balance method for rotor/stator interactions. *J Turbomach* 2012;**134**(1):011001.
9. He L, Ning W. Efficient approach for analysis of unsteady viscous flows in turbomachines. *AIAA J* 1998;**36**(11):2005–12.
10. Yi J, He L. Space–time gradient method for unsteady bladerow interaction—Part I: Basic methodology and verification. *J Turbomach* 2015;**137**(11):111008.
11. He L, Yi J, Adami P, et al. Space–time gradient method for unsteady bladerow interaction—Part II: Further validation, clocking, and multidisturbance effect. *J Turbomach* 2015;**137**(12):121004.
12. Wang DX, Huang XQ. Solution stabilization and convergence acceleration for the harmonic balance equation system. *J Eng Gas Turbines Power* 2017;**139**(9):092503.
13. Huang XQ, Wu HK, Wang DX. Implicit solution of harmonic balance equation system using the LU-SGS method and one-step Jacobi/Gauss-Seidel iteration. *Int J Comput Fluid Dyn* 2018;**32**(4–5):218–32.
14. Zhang HM, Wang DX. Time vector marching method for analyzing complex periodic unsteady flows within turbomachinery. *J Propuls Power* 2021;**37**(1):108–25.
15. Liu YW, Lu LP, Fang L, et al. Modification of Spalart-Allmaras model with consideration of turbulence energy backscatter using velocity helicity. *Phys Lett A* 2011;**375**(24):2377–81.
16. Jameson A, Schmidt W, Turkel E. Numerical solution of the Euler equations by finite volume methods using Runge Kutta time stepping schemes. Reston: AIAA; 1981. Report No.: AIAA-1981-1259.
17. Yoon S, Jameson A. Lower-upper Symmetric-Gauss-Seidel method for the Euler and Navier-Stokes equations. *AIAA J* 1988;**26**(9):1025–6.
18. Reid L, Moore RD. Design and overall performance of four highly loaded, high speed inlet stages for an advanced high-pressure-ratio core compressor. Washington, D.C.: NASA;1978. Report No.: 1337.
19. Reid L, Moore RD. Performance of single-stage axial-flow transonic compressor with rotor and stator aspect ratios of 1.19 and 1.26, respectively, and with design pressure ratio of 1.82. Washington, D.C.: NASA; 1978. Report No.: 1338.
20. Wang DX, Huang XQ. A complete rotor-stator coupling method for frequency domain analysis of turbomachinery unsteady flow. *Aerosp Sci Technol* 2017;**70**:367–77.